A pure inorganic 2-D framework based on paradodecatungstate and Mn^{2+} ions: syntheses, structure, and properties

Lizhou Wu, Wen Yang, Xinbo Dong, Chengxing Yu, Bin Liu, Yonghong Yan, Huaiming Hu & Ganglin Xue

View supplementary material 🔗

Accepted author version posted online: 13 May 2015.
Published online: 22 Jun 2015.

Submit your article to this journal 🔗

Article views: 58

View related articles 🔗

View Crossmark data 🔗

Taylor & Francis
Taylor & Francis Group

A pure inorganic 2-D framework based on paradodecatungstate and Mn²⁺ ions: syntheses, structure, and properties

LIZHOU WU†‡, WEN YANG†, XINBO DONG†, CHENGXING YU†, BIN LIU†, YONGHONG YAN†, HUAIMING HU† and GANGLIN XUE*†

†Key Laboratory of Synthetic and Natural Functional Molecule Chemistry of the Ministry of Education, Department of Chemistry, Northwest University, Xi'an, PR China
‡Department of Chemistry and Chemical Engineering, Ankang University, Ankang, PR China
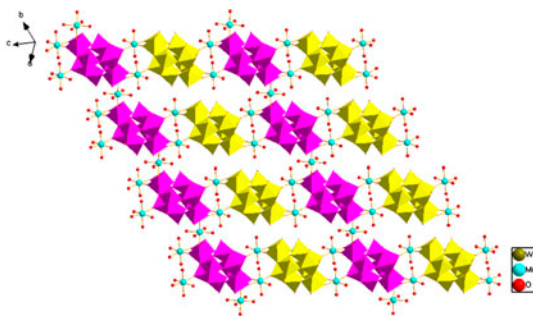
The pure inorganic–inorganic hybrid represents an extended structure constructed from paradodecatungstate and transition metal ions and shows definite catalytic activities on the probe reaction of benzyl alcohol oxidation to benzaldehyde with H_2O_2.

A pure inorganic 2-D framework based on paradodecatungstate polyanions and $[Mn(H_2O)_n]^{2+}$ ($n = 2$, 3) ions, $Na_{10}\{[Mn(H_2O)_3]_2[H_2W_{12}O_{42}]\}\{[Mn(H_2O)_3]_2[Mn(H_2O)_4][H_2W_{12}O_{42}]\}\cdot56H_2O$ (**1**), has been synthesized and characterized by IR spectra, UV–vis spectra, thermogravimetric analysis (TGA), single-crystal X-ray diffraction, and magnetic measurements. Single-crystal X-ray diffraction analysis indicates that $[H_2W_{12}O_{42}]^{10-}$ in **1** is a tetradentate ligand and coordinates to four $[(Mn(H_2O)_3]^{2+}$ cations through terminal oxygens to form manganese doubly bridged 1-D chains, which are further linked through $[Mn(H_2O)_4]^{2+}$ ions into a 2-D layer. The catalytic activities of **1** are tested in the selective oxidation of benzyl alcohol to benzaldehyde with 30% aqueous H_2O_2 as oxidant in toluene, exhibiting 90% conversion and 93% selectivity. Magnetic studies indicate that weak antiferromagnetic couplings exist between the Mn(II) ions in **1**.

Keywords: Polyoxometalate; Paradodecatungstate; Two-dimensional layer; Catalytic oxidation; Magnetic property

---

*Corresponding author. Email: glxue@nwu.edu.cn

1. Introduction

Organic–inorganic and inorganic–inorganic hybrids are important classes of materials and these different components often have multiple functionalities, such as catalysis, electrochemistry, biochemistry, photochemistry, and magnetism [1–8]. Polyoxometalates (POMs) are a fascinating class of metal–oxygen cluster compounds with diverse properties and have been viewed as ideal inorganic building blocks to construct POM-supported functional ensembles [9, 10]. The design and construction of high-dimensional POMs hybrids have become a major research area in POM chemistry [11–14]. The paradodecatungstate cluster $[H_2W_{12}O_{42}]^{10-}$ possesses 36 potentially coordinating oxygens and relatively high charge density that make the surface oxygens activated to form high-dimensional covalent networks [15–18]. Dozens of examples utilizing this anion to construct extended structures have been reported, such as 1-D structures in which the paradodecatungstate is bidentate or tetradentate coordinating to the hetero-metal groups, $[Mn_4(H_2O)_{14}(H_2W_{12}O_{42})]^{2-}$ [15], $[\{Cd(H_2O)_2\}(H_2W_{12}O_{42})]^{8-}$ [17], $[\{Cu(en)_2\}_2(H_2W_{12}O_{42})]^{6-}$ [19], $[Bi(H_2W_{12}O_{42})]^{7-}$ [20], $[Mn(H_2O)_2(H_2W_{12}O_{42})]^{8-}$ [21], $[Mn_2(H_2O)_8(H_2W_{12}O_{42})]^{6-}$ [22]; 2-D layer-like structures linked with six or eight heterometal groups, $\{[Co(H_2O)_3][Co(H_2O)_4][H_2W_{12}O_{42}]\}^{6-}$ [17], $[Zn_4(H_2O)_{14}(H_2W_{12}O_{42})]^{2-}$ [21], $[Cd(H_2O)_2(H_2W_{12}O_{42})]^{8-}$ [23], $\{[Cu(en)_2]_3[H_2W_{12}O_{42}]\}^{4-}$ [24], $[Cu(en)_2]_4[H_4W_{12}O_{42}]\cdot9H_2O$ [25], $[\{Cu(gly)(H_2O)\}]_2\{[Cu(H_2O)\}(H_2W_{12}O_{42})]^{6-}$ [26]; and 3-D structures held together through six, eight, or ten heterometal groups, $\{[Co(H_2O)_4]_3[H_2W_{12}O_{42}]\}^{4-}$ [17], $[Co_5(H_2O)_{22}][H_2W_{12}O_{42}]\cdot12H_2O$ [18], $[\{Cu(en)\}_2H_2W_{12}O_{42}]^{6-}$ [24], $\{[Co(H_2O)_4]_2[H_2W_{12}O_{42}]\}^{6-}$ [27], $\{[Cu(en)_2]_3[H_2W_{12}O_{42}]\}^{4-}$ [28], $[\{Cu_{0.5}(H_2O)\}_4\{Cu_{0.5}(H_2O)_{1.5}\}_2(H_4W_{12}O_{42})]^{2-}$ [29], and $[\{Mn(H_2O)_3\}_2\{Mn(H_2O)_4\}_2(H_2W_{12}O_{42})]^{2-}$ [30]. The applications of paradodecatungstates are mainly in photochemistry, electrochemistry, and magnetism [17, 21, 23, 30–32]; reports on their catalysis are very limited. Krebs *et al.* used $[Na_2Co_2H_2W_{12}O_{42}(H_2O)_{12}]^{4-}$ and $[NaCo_3H_2W_{12}O_{42}(H_2O)_{16}]^{3-}$ as catalysts for oxidation of alcohols with about 46% conversion [16]. Lin *et al.* reported that $[\{Cu(en)_2\}_2(H_2W_{12}O_{42})]^{6-}$ has good catalytic activity for oxidation of cyclohexane to cyclohexanone with 36% conversion and 71% selectivity [19]. Herein, we report a new 2-D layer based on the paradodecatungstate unit $[H_2W_{12}O_{42}]^{10-}$ and $[Mn(H_2O)_n]^{2+}$ ($n = 3$, 4), $Na_{10}\{[Mn(H_2O)_3]_2[H_2W_{12}O_{42}]\}\{[Mn(H_2O)_3]_2[Mn(H_2O)_4][H_2W_{12}O_{42}]\}\cdot56H_2O$ ($W_{12}Mn_5$) (1). The catalytic activities of 1 are tested in the selective oxidation of benzyl alcohol to benzaldehyde with 30% aqueous H_2O_2 as oxidant in toluene.

2. Experimental

2.1. *Materials and methods*

All reagents were used without purification. IR spectra were recorded on an EQUINOX55 spectrometer on KBr pellets from 4000 to 400 cm^{-1}. Na, Mn, and Mo were analyzed on an IRIS Advantage ICP atomic emission spectrometer. UV spectra were performed on a Shimadzu UV-2550 spectrophotometer. Thermogravimetric analysis was performed on a model Q600SDT analyzer in flowing N_2 with a heating rate of 10 °C min^{-1}. The X-ray powder diffraction (XRPD) data were recorded on a Rigaku RU200 diffractometer at 60 kV, 300 mA, and Cu Kα radiation ($\lambda = 1.5406$ Å), with a scan speed of 5° min^{-1} and a step size of 0.02° in 2θ. Magnetic measurements were obtained on polycrystalline 1 18.57 mg using a

Quantum Design MPMS-XL7 SQUID magnetometer between 1.8 and 300 K for direct current (dc). Catalytic reactions were monitored using a GC, HP sp-6890 chromatogram.

2.2. Synthesis of $Na_{10}\{[Mn(H_2O)_3]_2[H_2W_{12}O_{42}]\}\{[Mn(H_2O)_3]_2[Mn(H_2O)_4][H_2W_{12}O_{42}]\}\cdot56H_2O$ (1)

The synthesis of **1** was accomplished by adding a solution of $MnSO_4\cdot H_2O$ (0.06 g, 0.25 mmol) dissolved in H_2O (20 mL) to a solution of $Na_2WO_4\cdot2H_2O$ (0.92 g, 3.0 mmol) dissolved in H_2O (20 mL) with vigorous stirring; the pH was adjusted to 4.5 with 4 M HCl. The solution was stirred at 80 °C for 2 h, then cooled to room temperature and filtered. After about one month, light yellow needle-like crystals were collected (yield: 0.27 g, 32% based on W). Elemental analysis calcd (%) for $Na_{10}Mn_5H_{148}O_{156}W_{24}$: Na, 3.04; Mn, 3.63; W, 58.35. Found (%): Na, 2.98; Mn, 3.70; W, 58.21.

2.3. Crystallographic structure determination

A suitable single crystal having approximate dimensions of 0.16 mm × 0.12 mm × 0.10 mm for **1** was mounted on a glass fiber capillary which was put on a BRUKER SMART APEX II CCD diffractometer. Data collection was performed at 293(2) K with graphite-monochromatic radiation Mo Kα ($\lambda = 0.71073$ Å). The structure was solved by direct methods (SHELXTL-97) and refined by full-matrix-block least-squares on F^2. Heavy atoms (W, Mn, and Na) were refined with anisotropic displacement parameters, and the oxygens were refined isotropically. Hydrogens were not included. Further details of the crystal

Table 1. Crystal data and structure refinement for **1**.

Empirical formula	$H_{148}Mn_5Na_{10}O_{156}W_{24}$
Formula weight	7562.18
T/K	293(2)
Crystal system	Triclinic
Space group	P-1
a/Å	12.4662(15)
b/Å	14.8683(19)
c/Å	19.071(2)
α/°	93.202(2)
β/°	101.104(2)
γ/°	94.067(2)
V/Å^3	3451.1(7)
Z	1
D_{calc}/g cm^{-3}	3.639
Absorption coefficient/mm^{-1}	20.510
Reflections measured	17,494
Independent reflections	12,050
Reflections used	7056
R_{int}	0.0294
GoF on F^2	1.007
$R1^a$ [$I > 2\sigma(I)$], $wR2^b$ [$I > 2\sigma(I)$]	0.0407, 0.1161
$R1^a$ (all data), $wR2^b$ (all data)	0.0705, 0.1479
$\Delta\rho$min/max (e/Å^3)	2.205 (0.84 Å from O60), −3.697 (0.51 Å from W3)

[a] $R1 = [\Sigma|F_o|-|F_c|]/[\Sigma|F_c|]$.

[b] $wR2 = \left\{ \left[\sum w\left(F_o^2 - F_c^2\right)^2 \right] / \left[\sum w\left(F_o^2\right)^2 \right] \right\}^{1/2}$.

structure investigation can be obtained from the Fachinformationszentrum Karlsruhe, 76344 Eggenstein-Leopoldshafen, Germany (Fax: (49)7247-808-666; E-mail: crysdata@fiz-karlsruhe.de) on quoting the depository number CSD-428477. A summary of the crystallographic data and structural determination for **1** is provided in table 1. Selected bond lengths and angles of **1** are listed in table S1 (see online supplemental material at http://dx.doi.org/10.1080/00958972.2015.1046851).

3. Results and discussion

3.1. *Crystal structure of 1*

Single-crystal X-ray diffraction analysis reveals that **1** crystallizes in the space group *P*-1, the asymmetric unit consisting of two half polyanions $[H_2W_{12}O_{42}]^{10-}$, half of a $[Mn(H_2O)_4]^{2+}$, two $[(Mn(H_2O)_3]^{2+}$ cations, five sodium cations, and 28 lattice water molecules (figure 1). The structure of the paradodecatungstate ion $[H_2W_{12}O_{42}]^{10-}$ is similar to those previously reported [33, 34], centrosymmetric with two W_3O_{13} triangular subunits and two open angular W_3O_{14} groups, held together through interconnecting corners into a cluster leaving a central cavity containing two disordered protons. The oxygens of $[H_2W_{12}O_{42}]^{10-}$ in **1** can be divided into four groups: (i) tungsten–terminal oxygen, 1.699–1.768 Å; (ii) tungsten–oxygen linked to manganese, 1.726–1.809 Å; (iii) tungsten–bridging oxygen, 1.789–2.206 Å; (iv) tungsten–internal oxygen common to three tungsten ions, 1.870–2.322 Å.

In **1**, there are two crystallographic types of $[H_2W_{12}O_{42}]^{10-}$ clusters, one hexadentate coordinating to four Mn^{2+} cations through six terminal oxygens of angular-type W_3O_{14} groups, and another as octadentate coordinating to six Mn^{2+} cations through eight terminal oxygens of triangular W_3O_{13} groups and angular W_3O_{14} groups. All crystallographically independent Mn centers (Mn1, Mn2, and Mn3) exhibit distorted octahedral geometry. Mn1 is coordinated with four oxygens from four coordinated waters and two oxygens from
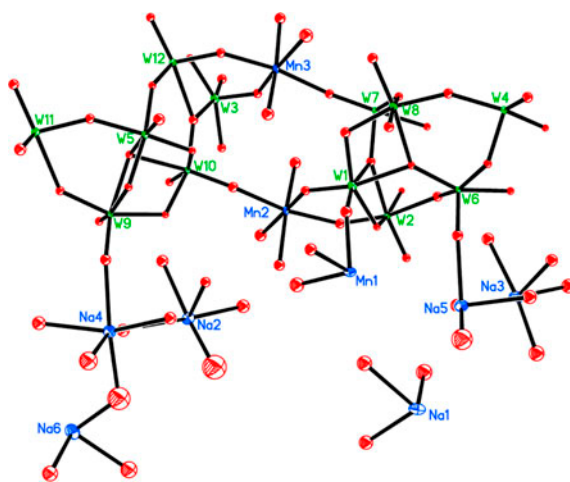

Figure 1. Displacement ellipsoid (30% probability) representation of the asymmetric unit of **1**; all lattice water molecules are omitted for clarity.
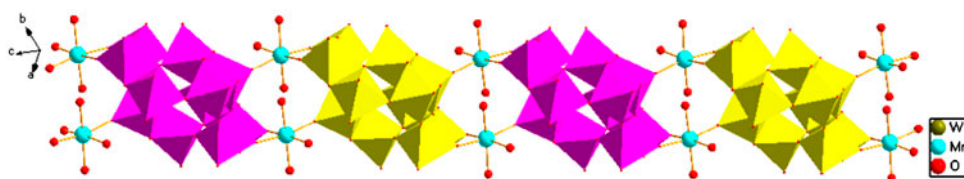
Figure 2.   Combined polyhedral/ball-and-stick representation of 1-D chain in **1**.

$\{W_3O_{14}\}$ subunits of two neighboring paradodecatungstate clusters (Mn–O, 1.926–2.409 Å). Mn2/Mn3 is coordinated by three oxygens from three coordinated waters, one oxygen from the triangular W_3O_{13} subunit of one cluster, and two oxygens from the open trimeric W_3O_{14} subunits of one other cluster (Mn–O, 1.925–2.516 Å).

The most remarkable structural feature of **1** is that adjacent paradodecatungstate $[H_2W_{12}O_{42}]^{10-}$ clusters are interconnected through double $[Mn(H_2O)_3]^{2+}$ bridging groups to form a 1-D anionic chain $\{[Mn(H_2O)_3]_2[H_2W_{12}O_{42}]\}_n^{6n-}$ along the [1 1 1] direction (figure 2), and the 1-D anionic chains $\{[Mn(H_2O)_3]_2[H_2W_{12}O_{42}]\}_n^{6n-}$ are linked by $[Mn(H_2O)_4]^{2+}$ cations to form 2-D layers in the (0 −1 1) plane as shown in the figure 3. To the best of our knowledge, no analogous extended structure consisting of this kind of POM has been reported. Neighboring layers are interconnected through Na–O slat bonds into a 3-D framework (figure S1).

3.2. Synthesis

The paradodecatungstate cluster $[H_2W_{12}O_{42}]^{10-}$ and $[Mn(H_2O)_n]^{2+}$ (n = 2, 3, 4) complexes can form a series of solid hybrids (figure 4). Compound **1** was synthesized by treating a
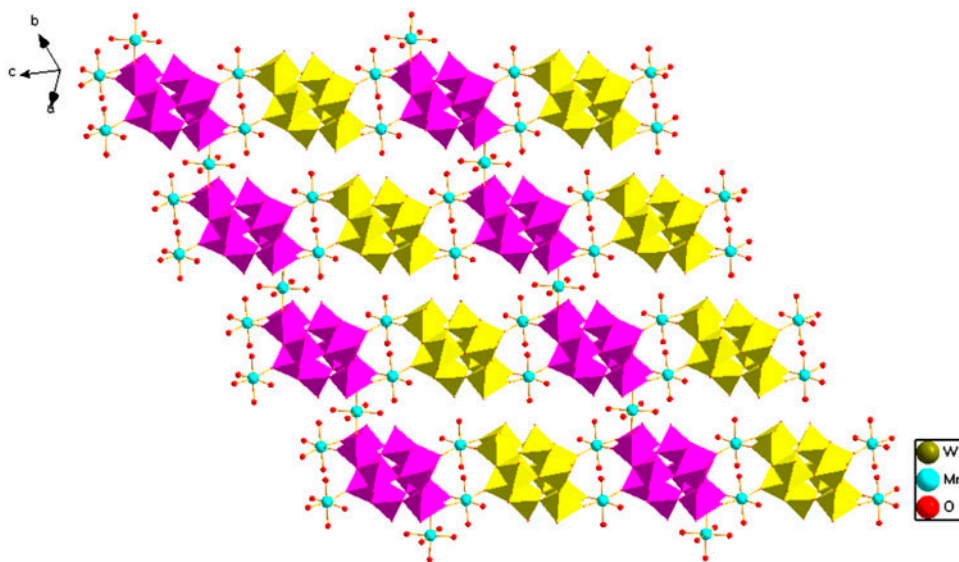

Figure 3.   Combined polyhedral/ball-and-stick representation of 2-D layers in **1**.
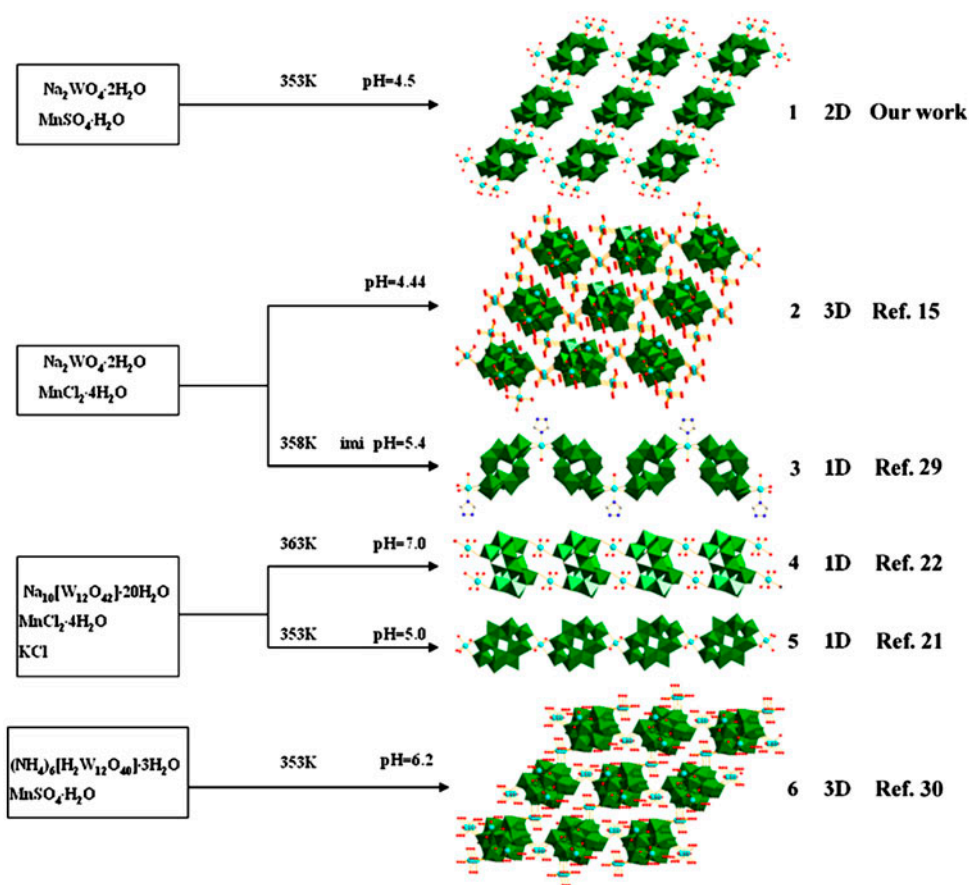
Figure 4. A series of polyoxometalates based on the paradodecatungstate cluster $[H_2W_{12}O_{42}]^{10-}$ and $[Mn(H_2O)_n]^{2+}$.

suspension of $Na_2WO_4 \cdot 2H_2O$ and $MnSO_4 \cdot H_2O$ at 80 °C in pH 4.5; the paradodecatungstate clusters in **1** are linked with four or six heterometal groups. Compounds **2** and **3** were obtained by mixture of $Na_2WO_4 \cdot 2H_2O$ and $MnCl_2 \cdot 4H_2O$. Compound **2** displays a 3-D framework at pH 4.44 [15] and **3** forms a 1-D chain at 85 °C in pH 5.4 [29]. Compounds **4** and **5** were prepared by mixture of $Na_{10}[W_{12}O_{42}] \cdot 20H_2O$, $MnCl_2 \cdot 4H_2O$, and KCl with pH values ranging from 5.0 to 7.0. Compound **4** was isolated at pH 7.0; the paradodecatungstate cluster in **4** is a tetradentate chelate ligand and bridges to two neighbors through four $[Mn(H_2O)_4]^{2+}$ complexes [22]. The paradodecatungstate cluster in **5** is bidentate, coordinated to two $[Mn(H_2O)_2]^{2+}$ ions to form a 1-D chain [21]. Compound **6** was obtained by mixture of $(NH_4)_6[H_2W_{12}O_{40}] \cdot 20H_2O$ and $MnSO_4 \cdot H_2O$ with molar ratio of 10 : 3 at 80 °C in pH 6.2; the paradodecatungstate cluster in **6** is held together through eight heterometal groups into a 3-D structure [30]. The species and configurations of final products depend on many factors, such as pH, reaction temperature, initial reactants, stoichiometric ratio, organic ligands, counter cations, etc. and systematic exploration on this system still remains a challenge.

3.3. *IR and thermal analyses*

In the IR spectrum (figure S2) of **1**, peaks at 940, 862, 806, 700, and 496 cm^{-1} can be attributed to v_{as}(W=O$_t$), v_{as}(W–O$_b$–W), v_{as}(W–O$_c$–W), and v_{as}(Mn–O) vibration modes, and those at 3420 and 1624 cm^{-1} can be attributed to the stretching modes of crystallization and coordination water molecules, which are consistent with the result of single-crystal X-ray diffraction analysis. According to the TG curve of **1** (figure S3), the thermal decomposition is divided into two steps. First, it gradually loses all lattice and coordinated water molecules from 32 to 310 °C, with a weight loss of 16.9% (calculated value of 17.0%). The second weight loss of 0.5% (calc. 0.6%) at 310–600 °C is ascribed to decomposition of the polyanion framework structure. The final product should be the mixed metal oxide $Mn_5Na_{10}O_{82}W_{24}$, and the whole weight loss of 17.4% is in agreement with the calculated value of 17.6%. The DSC curve shows three endothermic peaks at ~59, ~123, and ~320 °C corresponding to loss of all lattice water, coordinated water molecules, and the decomposition of the polyanion framework structure.

3.4. *UV and XRD analyses*

In the UV region, **1** exhibits two characteristic bands for the ligand to metal charge transfer in the polyanions (figure S4). The more intense band corresponding to p$_\pi$ (O$_d$) → d$_{\pi*}$ (W) transitions [35] is at 194.0 nm. The broader band around 247.0 nm is assigned to the p$_\pi$ (O$_{b,c}$) → d$_{\pi*}$ (W) charge transfer transition in the tricentric bonds of POMs, consistent with the literature values (193.6 and 250.7 nm) [36]. The powder XRD pattern of **1** and the simulated XRD pattern are shown in Supplemental data (figure S5) and the diffraction peaks on the pattern correspond well in position, confirming that the product is a pure phase. The differences in reflected intensity are probably due to preferred orientation in the powder samples.

3.5. *Magnetic properties*

Figure 5 shows the experimental data of **1** plotted as $\chi_M T$ *versus* T and $1/\chi_M$ *versus* T. The $\chi_M T$ value of 21.78 cm^3 K mol^{-1} at 300 K is in agreement with the spin-only value of
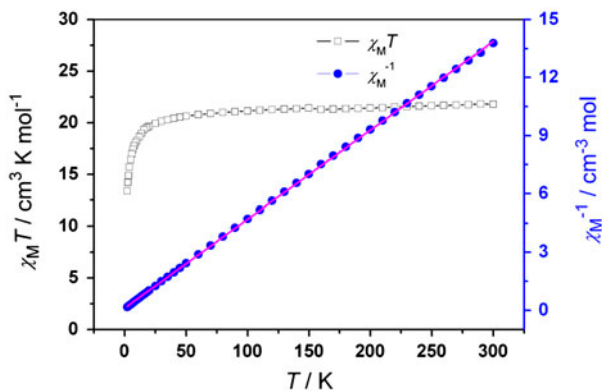

Figure 5.   Temperature dependence of $\chi_M T$ and χ_M^{-1} for **1**.

21.87 cm^3 K mol^{-1} for five noninteracting Mn^{II} ions ($g = 2$, $S = 5/2$). The $\chi_M T$ decreases continuously with decreasing temperature. Below 20 K, $\chi_M T$ quickly decreases and reaches a minimum value of 13.30 cm^3 K mol^{-1} at 2.0 K. This behavior indicates the presence of weak antiferromagnetic interactions between the Mn^{II} ions. The $1/\chi_M$ *versus T* curve is in accord with the Curie–Weiss law with $C = 21.80$ cm^3 K mol^{-1} and $\theta = -2.4$ K. The negative Weiss constant further demonstrates antiferromagnetic interactions between the Mn^{II} ions through oxygen bridges. The antiferromagnetic exchange interactions of the manganese containing paradodecatungstate have been observed in previous studies [15, 21]. For instance, the aniferromagnetic manganese containing paradodecatungstate Na$_2$[Mn$_4$(H$_2$O)$_{14}$(H$_2$W$_{12}$O$_{42}$)]·16H$_2$O has been isolated by Ni *et al.* [15].

3.6. *Catalytic properties*

The selective oxidation of benzyl alcohol to benzaldehyde with 30% H$_2$O$_2$ was carried out to investigate the oxidative catalytic activity of **1**. The reaction conditions are the same as previously reported [37]. In a typical experiment, a reaction mixture containing 5 mL toluene as solvent, 0.43 g of benzyl alcohol, 0.05 g of catalyst, and excess of H$_2$O$_2$ (H$_2$O$_2$/benzyl alcohol = 5) was heated to 80 °C and kept at this temperature for 8 h with constant stirring. As shown in table 2, hydrogen peroxide, alone, is almost unable to oxidize the substrate in the absence of any catalyst (entry 1). Compound **1** (W$_{12}$Mn$_5$) exhibits higher activity and selectivity (90% conversion and 93% selectivity) than MnCl$_2$ or (NH$_4$)$_{10}$[H$_2$W$_{12}$O$_{42}$]·6H$_2$O (only 46 or 58% conversion and 55 or 82 selectivity). The results indicate that the introduction of Mn^{2+} into the paradodecatungstate framework of [H$_2$W$_{12}$O$_{42}$]$^{10-}$ is beneficial for catalysis. Just like the introduction of two vanadium ions into the Keggin framework [PW$_{12}$O$_{40}$]$^{3-}$, the bisvanadium-substituted heteropolyoxometalate catalyst H$_5$[PV$_2$W$_{10}$O$_{40}$]/MCM-41/NH$_2$ exhibits higher activity than saturated heteropolyoxometalate catalyst H$_3$[PW$_{12}$O$_{40}$]/MCM-41/NH$_2$ in the oxidation of benzyl alcohol to benzaldehyde (entries 5 and 6) [37]. In some catalytic systems, it was difficult to control the production of benzaldehyde in the oxidation of benzyl alcohol, and often benzoic acid was obtained instead of benzaldehyde. Na$_{12}$[WZnZn$_2$(H$_2$O)$_2$(ZnW$_9$O$_{34}$)$_2$] [38] oxidized primary alcohols to the corresponding carboxylic acid, including benzyl alcohol. Another catalyst, Na$_6$[SiW$_{11}$ZnH$_2$O$_{40}$]·12H$_2$O [39], showed high activity in oxidation of benzyl alcohol, but the product was also benzoic acid. The good activity and selectivity of W$_{12}$Mn$_5$ may be attributed to the following reasons: (1) the cooperative action of the manganese center and the tungsten ions in paradodecatungstate skeleton and the synergetic interactions between Mn^{2+} and [H$_2$W$_{12}$O$_{42}$]$^{10-}$ polyanion; (2) the coordination environment

Table 2. Oxidation of benzyl alcohol into benzaldehyde by various catalysts.

Entry	Catalyst	Time (h)	Conversion (%)	Selectivity (%)
1	No catalyst	8	5	100
2	MnCl$_2$	8	46	55
3	(NH$_4$)$_{10}$[H$_2$W$_{12}$O$_{42}$]·6H$_2$O	8	58	82
4	Compound **1** (W$_{12}$Mn$_5$)	8	90	93
5	H$_3$[PW$_{12}$O$_{40}$]/MCM-41/NH$_2^{37}$	8	70	87
6	H$_5$[PV$_2$W$_{10}$O$_{40}$]/MCM-41/NH$_2^{37}$	8	97	99
7	W$_{12}$Mn$_5$ after the fourth run	8	82	90

Note: Reaction condition: alcohol 0.43 g, catalyst 0.05 g, H$_2$O$_2$/benzyl alcohol = 5, toluene 5 ml, 80 °C for 8 h.

of manganese(II) ions. Based on its crystal structural analysis, the crystal structure of **1** contains a 2-D anionic layer $\{[Mn(H_2O)_3]_2[H_2W_{12}O_{42}]\}\{[Mn(H_2O)_3]_2[Mn(H_2O)_4]$ $[H_2W_{12}O_{42}]\}_n^{10n-}$; this structure may make Mn active sites more accessible with substrate molecules on both sides. The recyclability of $W_{12}Mn_5$ catalyst could be easily carried out by a simple procedure. For example, in the oxidation of benzyl alcohol, the benzaldehyde could be decanted from the biphasic system. We can isolate the $W_{12}Mn_5$ residue after completion of the reaction by evaporation of the water phase. The remaining $W_{12}Mn_5$ residue was therefore recharged with benzyl alcohol and hydrogen peroxide as above. Reaction workup was carried out again. We found that the reaction was carried out four times in consecutive runs with approximately 10% decrease in activity (entry 7). The fresh catalysts and the recycled catalysts after the fourth run were characterized with FT-IR spectra (figure S6). IR spectra of the fresh and recycled catalysts are very similar, suggesting that structure of recycled catalysts do not change and that they are stable and can be reused in the next reaction.

4. Conclusion

A polyoxometalate constructed from paradodecatungstate clusters $[H_2W_{12}O_{42}]^{10-}$ and $[Mn(H_2O)_n]^{2+}$ ($n = 3, 4$) has been synthesized by a conventional method. Single-crystal X-ray diffraction analysis indicates that $[H_2W_{12}O_{42}]^{10-}$ of **1** is tetradentate coordinating to four $[(Mn(H_2O)_3]^{2+}$ cations through the terminal oxygens to form unprecedented manganese doubly bridged 1-D chains, which are further linked through $[Mn(H_2O)_4]^{2+}$ into a 2-D layer. The catalytic performance of **1** shows efficient selective oxidation of benzyl alcohol to benzaldehyde with 90% benzyl alcohol conversion and 93% benzaldehyde selectivity.

Disclosure statement

No potential conflict of interest was reported by the authors.

Funding

References

[1] A.K. Cheetham. *Science*, **264**, 794 (1994).
[2] A. Müller, H. Reuter, S. Dillinger. *Angew. Chem. Int. Ed. Engl.*, **34**, 2328 (1995).
[3] M.T. Pope, A. Müller. *Angew. Chem. Int. Ed. Engl.*, **30**, 34 (1991).
[4] P.J. Hagrman, D. Hagrman, J. Zubieta. *Angew. Chem. Int. Ed.*, **38**, 2638 (1999).
[5] A. Müller, F. Peters, M.T. Pope, D. Gatteschi. *Chem. Rev.*, **98**, 239 (1998).
[6] C. Sanchez, P. Belleville, M. Popall, L. Nicole. *Chem. Soc. Rev.*, **40**, 696 (2011).
[7] C. Sanchez, K.J. Shea, S. Kitagawa. *Chem. Soc. Rev.*, **40**, 471 (2011).
[8] A. Dolbecq, E. Dumas, C.R. Mayer, P. Mialane. *Chem. Rev.*, **110**, 6009 (2010).
[9] C.L. Hill. *Chem. Rev.*, **98**, 1 (1998).
[10] D.L. Long, R. Tsunashima, L. Cronin. *Angew. Chem. Int. Ed.*, **49**, 1736 (2010).
[11] S.B. Li, H.Y. Ma, H.J. Pang, L. Zhang. *Cryst. Growth Des.*, **14**, 4450 (2014).

[12] L.L. Li, B. Liu, G.L. Xue, H.M. Hu, F. Fu, J.W. Wang. *Cryst. Growth Des.*, **9**, 5206 (2009).
[13] T.T. Yu, H.Y. Ma, C.J. Zhang, H.J. Pang, S.B. Li, H. Liu. *Dalton Trans.*, **42**, 16328 (2013).
[14] M.I. Khan, E. Yohannes, R.J. Doedens. *Inorg. Chem.*, **42**, 3125 (2003).
[15] X.T. Zhang, J.M. Dou, D.Q. Wang, Y.X. Zhang, Y. Zhou, R.J. Li, S.S. Yan, Z.H. Ni, J.Z. Jiang. *Cryst. Growth Des.*, **7**, 1699 (2007).
[16] I. Loose, M. Bösing, R. Klein, B. Krebs, R.P. Schulz, B. Scharbert. *Inorg. Chim. Acta*, **263**, 99 (1997).
[17] C.Y. Sun, S.X. Liu, L.H. Xie, C.L. Wang, B. Gao, C.D. Zhang, Z.M. Su. *J. Solid State Chem.*, **179**, 2093 (2006).
[18] Z. Žák, J. Perůtka, J. Havel, I. Císařová, G. Giester. *J. Alloys Compd.*, **281**, 169 (1998).
[19] B.Z. Lin, Y.M. Chen, P.D. Liu. *Dalton Trans.*, **12**, 2474 (2003).
[20] Z.-H. Xu, X.-L. Wang, Y.-G. Li, E.-B. Wang, C. Qin, Y.-L. Si. *Inorg. Chem. Commun.*, **10**, 276 (2007).
[21] L. Yuan, C. Qin, X.L. Wang, E.B. Wang, Y.G. Li. *Solid State Sci.*, **10**, 967 (2008).
[22] X. Gan, Z.M. Zhang, E.B. Wang. *Chem. J. Chin. U.*, **28**, 2242 (2007).
[23] B. Li, L.H. Bi, W. Li, L.X. Wu. *J. Solid State Chem.*, **181**, 3337 (2008).
[24] L. Lisnard, A. Dolbecq, P. Mialane, J. Marrot, F. Sécheresse. *Inorg. Chim. Acta*, **357**, 845 (2004).
[25] L.-W. He, B.-Z. Lin, X.-Z. Liu, X.-F. Huang, Y.-L. Feng. *Solid State Sci.*, **10**, 237 (2008).
[26] Y. Zhong, H. Fu, J.X. Meng, E.B. Wang. *J. Coord. Chem.*, **63**, 26 (2010).
[27] J.P. Wang, Q. Ren, J.W. Zhao, J.Y. Niu. *Chin. J. Struct. Chem.*, **25**, 1167 (2006).
[28] Y.Y. Li, C.L. Leng, J.W. Zhao, S.D. Chen, P.T. Ma, L.J. Chen. *Inorg. Chem. Commun.*, **25**, 35 (2012).
[29] S. Gao, J.X. Zhao, B.B. Zhou, K. Yu, Z.H. Su, L. Wang, Y.K. Yin, Z.F. Zhao, Y. Yu, Y. Chen. *Inorg. Chim. Acta*, **379**, 151 (2011).
[30] Q.-J. Kong, C.-J. Zhang, Y.-G. Chen. *J. Mol. Struct.*, **964**, 82 (2010).
[31] K.Y. Cui, F.Y. Li, L. Xu, Y.C. Wang, Z.X. Sun, H.G. Fu. *CrystEngComm*, **15**, 4721 (2013).
[32] H.J. Jeong, B.-I. Lee, S.-H. Byeon. *Dalton Trans.*, **41**, 14055 (2012).
[33] H.T. Evans Jr., *Acta Crystallogr., Sect. B: Struct. Crystallogr. Cryst. Chem.*, **32**, 1565 (1976).
[34] H.T. Evans Jr., U. Kortz, G.B. Jameson. *Acta Crystallogr., Sect. C: Cryst. Struct. Commun.*, **49**, 856 (1993).
[35] T. Yamase. *Chem. Rev.*, **98**, 307 (1998).
[36] D. Rusu, C. Craciun, A.L. Barra, L. David, M. Rusu, C. Rosu, O. Cozar, G. Marcu. *J. Chem. Soc., Dalton Trans.*, 2879 (2001).
[37] X.B. Dong, D.J. Wang, K.B. Li, Y.Z. Zhen, H.M. Hu, G.L. Xue. *Mater. Res. Bull.*, **57**, 210 (2014).
[38] D.S. Sloboda-Rozner, P.L. Alsters, R. Neumann. *J. Am. Chem. Soc.*, **125**, 5280 (2003).
[39] J.M. Wang, L. Yan, G.X. Li, X.L. Wang, Y. Ding, J.S. Suo. *Tetrahedron Lett.*, **46**, 7023 (2005).